



OPEN

Electrochemical generation of phenothiazin-5-ium. A sustainable strategy for the synthesis of new bis(phenylsulfonyl)-10*H*-phenothiazine derivatives

Niloofer Mohamadighader, Faezeh Zivari-Moshfegh & Davood Nematollahi  

In this work, the electrochemical generation of phenothiazin-5-ium (PTZ_{ox}) from the direct oxidation of phenothiazine (PTZ) in a water/acetonitrile mixture using a commercial carbon anode and conventional stainless steel cathode is reported. PTZ_{ox} is a reactive intermediate with high potential synthetic applications, which is used in this paper for the synthesis of new phenothiazine derivatives. In this work a novel and simple electrochemical methodology for the synthesis of some bis(phenylsulfonyl)-10*H*-phenothiazine derivatives was established. In this paper, a mechanism for PTZ oxidation in the presence of arylsulfonic acids has been proposed based on the results obtained from voltammetric and coulometric experiments as well as spectroscopic data of the products. These syntheses are performed in a simple cell by applying constant current under mild conditions and at room temperature with high atom economy.

Electrochemistry is a powerful tool to identify the mechanism of reactions as well as the synthesis of organic and inorganic compounds^{1–3}. In this research, we deal with three categories of compounds with valuable medicinal properties. The first category involves phenothiazines. Phenothiazine has various biological activities, such as neuroleptic, antiemetic and anti-histaminic activities, which have made it interesting to scientists⁴. Phenothiazine derivatives are also used as anti-cancer, antipyretic, anticonvulsant, analgesic, anti-fungal, anti-bacterial, anti-malarial, anti-inflammatory, and immunosuppressive agents^{4–6}. Prominent examples of widely used phenothiazine derivatives include trifluorophenazine, chlorpromazine, thioridazine, fluphenazine and perphenazine (Fig. 1, top row). From the electrochemical point of view, phenothiazine is a useful compound in photovoltaic⁷ and electrochemical applications^{8–11}. Also due to their interesting chemical and physical properties, phenothiazines are an important and widely used building block for a wide range of applications in different fields of chemistry¹². For example, these compounds are widely used in the optoelectronic industry due to the presence of electron-rich nitrogen and sulfur atoms in their molecules¹³. Also, since phenothiazines have a reversible redox process with low oxidation potential, they are widely used in perovskite solar cells¹⁴.

The second category of compounds are sulfones. Sulfone drugs are useful to treat many diseases, like anti-inflammatory¹⁵, antimicrobial¹⁶, anti-cancer¹⁷, and anti-malaria¹⁸. Diarylsulfones are useful in biological fields and pharmaceutical aims as antifungal, antimicrobial, anticancer, antibacterial and HIV treatment agents and also can be used to prepare other drugs^{19,20}. Prominent examples of widely used sulfone and diarylsulfone drugs are shown in Fig. 1, middle row. The third category of compounds are sulfonamides. Sulfonamides are the antibiotics that are applied in to treat bacterial infections²¹. In addition, they are used as anti-cancer, anti-inflammatory and antiviral drugs^{22–26}. Additionally, type II diabetes treatment activity is reported from some of these organic drugs²⁷. Moreover various type of diseases such as coronary artery disease, asthma²⁸, Alzheimer's²⁹ and respiratory diseases³⁰ have been treated by sulfonamide drugs which are called sulfa drugs. Examples of the most commonly used sulfonamides are shown in Fig. 1, bottom row.

Faculty of Chemistry and Petroleum Sciences, Bu-Ali-Sina University, Hamedan 65174-38683, Iran. ✉email: nemat@basu.ac.ir; nematollahid@gmail.com

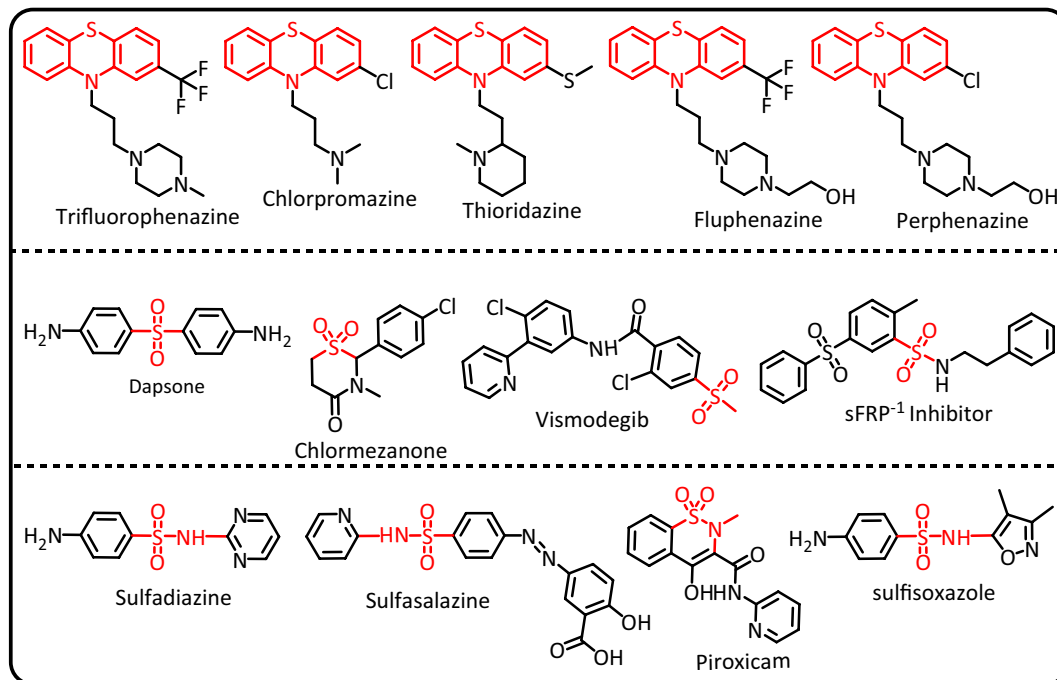


Figure 1. Examples of some biologically active phenthiazine, sulfone and sulfonamide drugs.

The medicinal properties of these three groups of compounds prompted us to prepare new molecules containing three moieties of phenthiazine, sulfone, and sulfonamide. The presence of these three moieties in one molecule can have high potential in variable medicinal and biological properties, and maybe the synergistic effect of these groups will intensify the medicinal properties and/or reduce the side effects of the synthesized molecule. To achieve this idea, the electrochemical oxidation of phenthiazine in the presence of some arylsulfonic acids has been carried out in an undivided cell using a carbon electrode. This work presents a sustainable and efficient one-step strategy with high atom economy under ambient conditions without using any catalyst for the synthesis of novel compounds with medicinal potential.

Experimental data

Apparatus and reagents

Voltammetric and controlled potential coulometric experiments were carried out using an Autolab model PGSTAT20 potentiostat/galvanostat (Metrohm-Autolab, Netherland) equipped with a working electrode (glassy carbon disc, 1.8 mm diameter), a counter electrode (platinum wire) and a reference electrode (Ag/AgCl) (3M KCl). All electrodes are prepared from Azar Electrode Company (Urmia, Iran). The alumina slurry from Iran Alumina Co. (0.1–3.0 μm) was used to polish the glassy carbon electrode. The working electrode (anode) used in macroscale electrolysis consists of a set of four soft carbon rods (diameter 8 mm and length 6 cm) placed at a distance of 3 cm from each other on the edges of a square. The counter electrode (cathode) consists of a stainless steel porous cylinder (area 25 cm^2) placed in the center of the square (Fig. 2). The electrolysis was carried out using a DC power supply model Dazheng ps-303D in an undivided cell equipped with a magnetic stirrer at room temperature. Controlled potential coulometry was performed in the same cell with an Ag/AgCl (3M KCl) reference electrode using a BEHPAJOOH-C2056 potentiostat.

Perkin-Elmer 1760 X device, German Bruker spectrometer (model: Avance 300 MHz), Agilent-5973C mass spectrometer and Barnstead Electrothermal 9100 instrument were used to record FTIR, NMR, MS spectra, and melting point, respectively. The NMR chemical shifts were related to the residual solvent signal. Phenthiazine (PTZ) and aryl sulfonic acid sodium salt, benzenesulfonic acid (BSA), 4-toluenesulfonic acid (TSA) and 4-chlorobenzenesulfonic acid (CSA) sodium salts were obtained from Sigma-Aldrich and used without further purification. The buffer solution with pH value of 2.0 was prepared by 0.2 M phosphoric acid (pro-analysis grade from E. Merck). The pH values were adjusted by sodium hydroxide.

General procedure for synthesis of bis(phenylsulfonyl)-10H-phenothiazine derivatives (2a–2e)

The electroorganic synthesis of bis(phenylsulfonyl)-10H-phenothiazine derivatives (2a–2e) has been carried out under controlled potential as well as constant current conditions at room temperature. In controlled potential electrolysis PTZ (0.25 mmol) and arylsulfonic acid (0.5 mmol) were electrolyzed at 0.55 V versus Ag/AgCl (3M KCl) in the mixture of water (phosphate buffer, pH 2.0, $c = 0.2$ M)/acetonitrile (50/50, v/v) (80 ml). The progress of the electrolysis was monitored by periodically recording the decrease of the oxidation peak current in cyclic voltammetry and also by using TLC on silica gel (ethyl acetate/*n*-hexane: 40/60). The samples on the TLC were visualized with a UV lamp (254 nm). To activate the electrode surface, the electrolysis is stopped for a while and

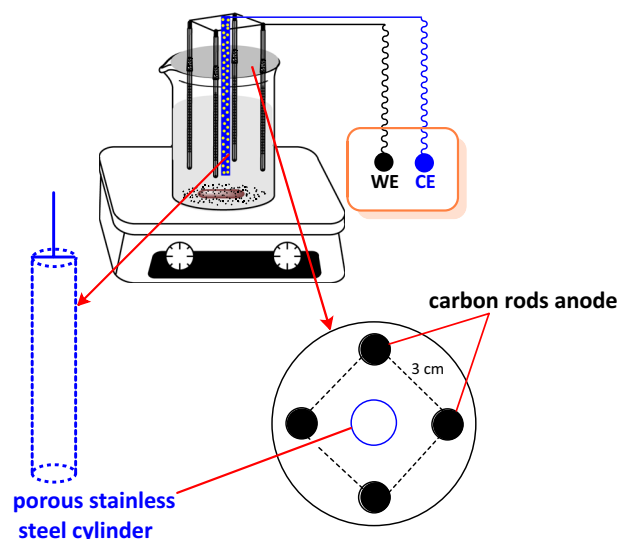
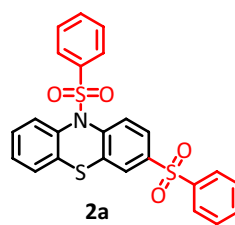


Figure 2. Cell used for the synthesis of phenothiazine derivatives.

the carbon anodes are washed with acetone. Electrolysis was terminated when the oxidation peak current reached 5% of the initial value. In this condition, the amount of electricity consumed is equal to 100 C. At the end of the electrolysis, the contents were placed at room temperature to reduce the volume of the solution (evaporation) to half and lead to the precipitation of the products. The crude precipitate was filtered and washed several times with water. After drying the product was purified by thin layer chromatography on silica gel GF250-60 with ethyl acetate/*n*-hexane (40/60 V/V). Product yield is calculated by weighing the pure product.

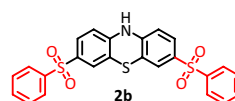
Electrolysis under constant current conditions has also been performed by applying a current density of 1.25 mA/cm² (30 mA) for 78 min (consumption of 140 C electricity) for oxidation of PTZ in the presence of BSA as well as other nucleophiles (TSA and CSA) under similar conditions as reported for electrolysis in controlled potential method.

Characteristics of the products



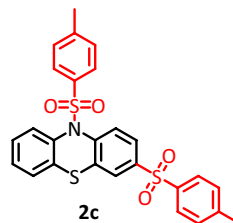
3,10-bis(phenylsulfonyl)-10H-phenothiazine (C₂₄H₁₉NO₄S₃) (2a)

Yellow powder (47.5 mg), isolated yield: 39%. Mp: 153–156 °C: ¹H NMR, δ ppm (300 MHz, DMSO-*d*₆), 6.2 (s, 1H, aromatic), 6.55 (d, *J* = 3.9 Hz, 2H, aromatic), 6.67–7.06 (m, 4H, aromatic), 7.49 (m, 7H, aromatic), 7.90 (d, *J* = 4.8 Hz, 3H, aromatic). ¹³C NMR, δ ppm (75 MHz, DMSO-*d*₆): 114.7, 115.9, 118.0, 123.6, 127.4, 127.6, 128.8, 129.7, 130.0, 130.2, 132.8, 133.7, 134.0, 134.4, 140.3, 142.4, 147.0. IR (KBr) (cm⁻¹): 2958, 2921, 2851, 1731, 1603, 1563, 1470, 1446, 1384, 1320, 1153, 1111, 1075, 722. MS (*m/z*) (EI, 70 eV) (relative intensity): 77 (30), 154 (40), 198 (90), 339 (100), 396 (20), 479 (M, 30).

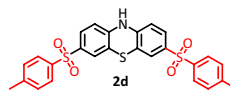


3,7-bis(phenylsulfonyl)-10H-phenothiazine ($C_{24}H_{19}NO_4S_3$) (**2b**)

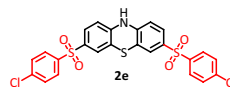
Cream powder (60.0 mg), isolated yield: 50%. Mp: 120–123 °C. 1H NMR, δ ppm (300 MHz, DMSO- d_6), 6.76 (d, $J=8.4$ Hz, 2H, aromatic), 7.46 (d, $J=5.3$ Hz, 2H, aromatic), 7.53 (d, $J=3.5$ Hz, 1H, aromatic), 7.55 (d, $J=2.1$ Hz, 1H, aromatic), 7.61 (d, $J=9.2$ Hz, 3H, aromatic), 7.66 (d, $J=6.7$ Hz, 2H, aromatic), 9.72 (s, 1H, NH). ^{13}C NMR, δ ppm (75 MHz, DMSO- d_6): 115.5, 117.7, 125.8, 127.5, 128.7, 130.1, 133.9, 135.0, 142.1, 145.0. UV_{max} (EtOH): 274 nm³¹. IR (KBr) (cm^{-1}): 3583, 3494, 3095, 2921, 1680, 1654, 1606, 1563, 1509, 1419, 1317, 1229, 1142, 745, 687.³¹ MS (m/z) (EI, 70 EV) (relative intensity): 77 (80), 107 (60), 291 (30), 338 (50), 396 (20), 479 (M, 100).

**3,10-ditosyl-10H-phenothiazine** ($C_{26}H_{21}NO_4S_3$) (**2c**)

Yellow powder (42.5 mg), isolated yield: 34%. Mp: 160–162 °C. 1H NMR, δ ppm (300 MHz, DMSO- d_6), 2.37 (s, 6H, CH₃), 6.68–7.04 (m, 4H, aromatic), 7.39 (d, $J=9.0$ Hz, 9H, aromatic), 7.50 (dd, $J=12.2$ Hz, 2H, aromatic), 7.80 (d, $J=8.1$ Hz, 3H, aromatic), 9.2 (s, 1H, aromatic). ^{13}C NMR, δ ppm (75 MHz, DMSO- d_6): 21.5, 114.6, 115.5, 115.9, 117.6, 117.9, 123.6, 125.6, 127.4, 128.4, 130.6, 133.8, 135.3, 139.2, 140.3, 144.5, 144.9, 146.8. IR (KBr) (cm^{-1}): 3053, 2958, 2921, 2851, 1703, 1630, 1600, 1534, 1499, 1438, 1347, 1297, 1260, 1113, 1019, 886, 770, 717. MS (m/z) (EI, 70 EV) (relative intensity): 55 (25), 91 (30), 154(30), 198 (60), 353 (100), 507 (M, 15).

**3,7-ditosyl-10H-phenothiazine** ($C_{26}H_{21}NO_4S_3$) (**2d**)

Cream powder (57.5 mg), isolated yield: 47%. Mp: 130–132 °C. 1H NMR, δ ppm (300 MHz, DMSO- d_6), 2.37 (s, 6H, CH₃), 6.67 (d, $J=6.9$ Hz, 1H, aromatic), 6.72 (d, $J=8.4$ Hz, 1H, aromatic), 6.82 (dd, $J=7.5$ Hz, 1H, aromatic), 6.92 (d, $J=7.8$ Hz, 1H, aromatic), 6.99 (d, $J=6.3$ Hz, 1H, aromatic), 7.04 (d, $J=7.8$ Hz, 1H, aromatic), 7.39 (m, $J=4.2$ Hz, 4H, aromatic), 7.79 (dd, $J=10.8$ Hz, 1H, aromatic), 7.78 (d, $J=8.1$ Hz, 3H, aromatic), 9.23 (s, 1H, NH). ^{13}C NMR, δ ppm (75 MHz, DMSO): 21.5, 114.6, 115.5, 115.8, 117.9, 123.6, 125.5, 126.8, 127.5, 128.2, 128.5, 130.5, 133.8, 139.6, 140.3, 144.3, 146.8. IR (KBr) (cm^{-1}): 3403, 3334, 3093, 2922, 2852, 1569, 1474, 1434, 1326, 1157, 1114, 1086, 828, 745, 616, 575. MS (m/z) (EI, 70 EV) (relative intensity): 65 (15), 91 (30), 154 (40), 198 (80), 353 (100), 507 (M, 10).

**3,7-bis((4-chlorophenyl) sulfonyl)-10H-phenothiazine** ($C_{24}H_{15}Cl_2NO_4S_3$) (**2e**)

Cream powder (67.5 mg), isolated yield: 50%. Mp: 145–148 °C. 1H NMR, (300 MHz, DMSO- d_6), 6.48 (d, $J=7.8$ Hz, 1H, aromatic), 6.54 (t, $J=8.4$ Hz, 2H, aromatic), 6.68 (d, $J=6.3$ Hz, 1H, aromatic), 6.77 (t, $J=7.8$ Hz, 1H, aromatic), 7.18 (d, $J=2.1$ Hz, 1H, aromatic), 7.29 (dd, $J=10.2$ Hz, 2H, aromatic), 7.43 (d, $J=8.4$ Hz, 3H, aromatic), 7.70 (d, $J=8.7$ Hz, 2H, aromatic), 9.36 (s, 1H, NH). ^{13}C NMR, δ ppm (75 MHz, DMSO): 114.7, 115.7, 115.8, 118.0, 123.6, 125.8, 126.7, 129.3, 130.2, 132.7, 138.7, 140.3, 141.4. IR (KBr) (cm^{-1}): 3438, 3028, 2918, 2850, 2709, 1578, 1566, 1457, 1223, 1155, 1121, 1009, 815, 682. MS (m/z) (EI, 70 EV) (relative intensity): 51 (35), 77 (45), 158 (40), 266 (50), 407 (100), 547 (M, 10).

Results and discussion**Electrochemical study of PTZ in the presence of arylsulfinic acids**

The cyclic voltammogram of PTZ (1.0 mM) in a solution of phosphate buffer 0.2 M, pH 2.0/ acetonitrile (50/50 v/v) in scan rate of 100 mV/s is shown in Fig. 3, part I, curve a. It reveals a quasi-reversible two-electron process involving oxidation of PTZ to phenothiazine-5-ime (PTZ_{ox}) (peak A₁ at 0.55 V vs. Ag/AgCl) and reduction of PTZ_{ox} to PTZ (peak C₁ at 0.45 V vs. Ag/AgCl)¹⁰. The peak current ratio (I_{PC1}/I_{PA1}) close to one which illustrates no side reaction is accrued in the time scale of voltammetry¹⁰. Figure 3, part I, curve b is the cyclic voltammogram of PTZ in the presence of 1.0 mM benzenesulfinic acid (BSA). Compared to cyclic voltammogram

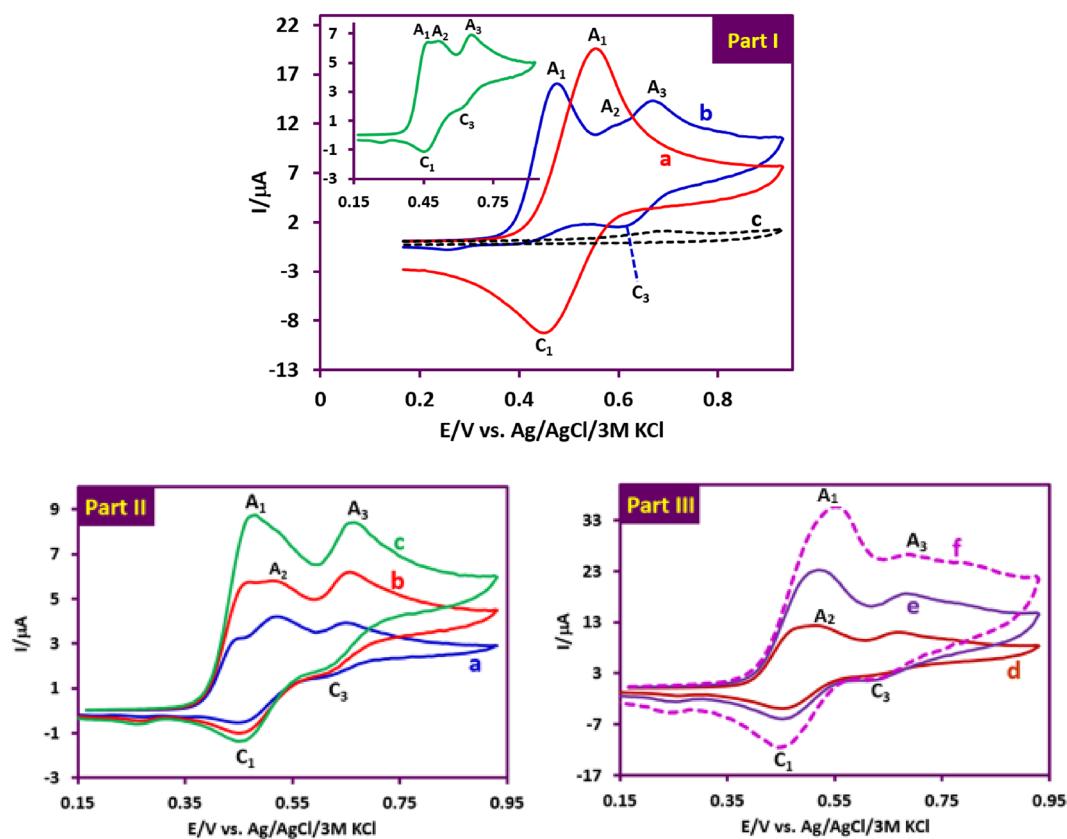


Figure 3. Part I: (a) Cyclic voltammogram of PTZ (1.0 mM). (b) Cyclic voltammogram of PTZ (1.0 mM) in the presence of 1.0 mM BSA. (c) Cyclic voltammogram of BSA (1.0 mM). Potential scan rate: 100 mV/s. inset: Cyclic voltammogram of PTZ (1.0 mM) in the presence of 0.5 mM BSA. Potential scan rate: 25 mV/s. Parts II and III: Cyclic voltammograms of PTZ (1.0 mM) in the presence of 0.5 mM BSA at different scan rates. Scan rates from a to f are: 10, 25, 50, 100, 300 and 500 mV/s. Solvent: phosphate buffer (pH 2.0, $c=0.2$ M)/acetonitrile mixture (50/50 v/v). All experiments were performed at room temperature using a GC electrode.

a, the following changes have occurred in the cyclic voltammogram of b. The first change is the removal of the cathode peak C_1 , which confirms the reaction between PTZ_{ox} and BSA. The second change is the appearance of an ill-defined irreversible peak A_2 and a new reversible redox peak (A_3 and C_3) at more positive potentials. The peak A_2 is related to the oxidation of the adduct formed from the reaction of PTZ_{ox} with BSA (PTZ -BSA) ($INT1_{ox}$) to $INT1_{ox}$ (Fig. 3, part I, curve b). The positive shift of peak A_2 compared to peak A_1 can be justified based on the electron withdrawing property of BSA bound to PTZ . After the electrochemical generation of $INT1_{ox}$, another rapid chemical reaction occurs and a BSA binds to $INT1_{ox}$. This chemical reaction causes the cathodic peak corresponding to the reduction of $INT1_{ox}$ (C_2) to be eliminated. Finally, the anodic and cathodic peaks A_3 and C_3 are related to the oxidation and reduction of final products (**2b**, **2d**, **2e**), respectively. The occurrence of oxidation of the final products at more positive potentials than the potential of peak A_2 confirms the presence of two BSA groups in the structure of the final products. The third change is the shift of E_{pA1} towards less positive potentials. This is another confirmation of the reaction between electrochemically generated PTZ_{ox} and BSA³².

In Fig. 3, part I, curve c is related to BSA in the absence of the PTZ . The peak observed in this cyclic voltammogram is attributed to the one electron oxidation of BSA to the corresponding radical³³. An important point regarding the peak current ratio (I_{pC1}/I_{pA1}) is the dependence on the nucleophile (BSA) concentration and on the potential scan rate. As shown in the Fig. 3, part I, inset, the peak current ratio (I_{pC1}/I_{pA1}) increases with decreasing BSA concentration. Comparison of this voltammogram with voltammogram b shows that decreasing the concentration of BSA slows down the reaction rate of BSA with PTZ_{ox} and leads to more PTZ_{ox} remaining on the electrode surface, which leads to an increase in the cathodic peak current (I_{pC1}). The effect of scan rate on the cyclic voltammograms of PTZ /BSA mixture is shown in Fig. 3, parts II and III. As can be seen, at low scan rates such as 10 mV/s (part II, curve a), peaks A_1 , A_2 , and A_3 are clearly observed in the anodic cycle, and peaks C_1 and C_3 are also observed in the cathodic scan. Increasing the potential scan rate causes remarkable two changes in the current of the peaks. The first change is related to the gradual decrease of the anodic peaks A_2 and A_3 with the increase of the scan rate and the second change is related to the increase of I_{pC1} with increasing scan rate. When the scan rate increases, there is not enough time for the BSA to react with PTZ_{ox} . In such a situation, most of the PTZ_{ox} molecules participate in the cathodic reaction, which results in an increase in I_{pC1} . On the one hand, the

current of anodic peaks A_2 and A_3 decrease, because these peaks are related to the oxidation of mono-substituted and di-substituted **PTZs**, respectively, which are not formed under these conditions.

Based on the obtained electrochemical data, the synthesis of bis(phenylsulfonyl)-10*H*-phenothiazine derivatives (**2a–e**) was carried out. The products after separation and purification were identified by various spectroscopic methods such as IR, NMR and MS. Based on spectroscopic data as well as voltammetric results, the following mechanism is proposed for the oxidation of **PTZ** in the presence of **BSA** (Fig. 4). This mechanism can be extended to other nucleophiles (4-toluenesulfinic acid, **TSA** and 4-chlorobenzenesulfinic acid, **CSA**). According to the proposed mechanism, initially **PTZ** is converted into its oxidized form (phenothiazin-5-ium, **PTZ_{ox}**) by losing two electrons and one proton. In the next step, **PTZ_{ox}** is attacked by anion resulting from deprotonation of arylsulfinic acids (RSO_2^-) and forms the first intermediate (**INT1**) [3-(arylsulfonyl)-10*H*-phenothiazine] after aromatization. It should be noted that the formation of other isomers of **INT1** is also possible. However, due to the presence of sulfonium atom in the structure of **PTZ_{ox}**, it is suggested that C3 atom is the most favorable site for nucleophilic attack of arylsulfinic acids.

The oxidation of **INT1** in the next step causes the formation of **INT1_{ox}**. There are a few important points regarding this step. First, unlike **PTZ**, whose two rings A and B are similar, **INT1** rings A and B are not the same, and due to the presence of an electron-withdrawing arylsulfonyl group in ring A, oxidation takes place on the B-ring. Like **PTZ_{ox}**, **INT1_{ox}** is attacked by another arylsulfinic anion, leading to the final product after aromatization (Fig. 4). As seen in Fig. 4, two types of products are formed in the reaction of arylsulfinic anion with **INT1_{ox}**. One of these products is formed by the attack of arylsulfinic anion on the nitrogen atom of **INT1_{ox}** (path I). This compound is a sulfone-sulfonamide product. The second product results from an attack similar to the first arylsulfinic attack (path II), which leads to the formation of the sulfone-sulfone product. These products were separated from each other by thin layer chromatography.

To further investigate the oxidation of **PTZ** in the presence of **BSA**, the double potential step chronoamperometry method was also used (Fig. 5). To achieve this goal, based on **PTZ** cyclic voltammogram (Fig. 3, part I, curve a), the electrode potential is changed from an initial value of 0.20 V to a potential of 0.55 V in the forward step (oxidation step) and then to 0.40 V in the reverse step (reduction step). The generated current was recorded for 12 s in both step. Figure 5 curve a shows the chronoamperometry of **PTZ** (1.0 mM) in phosphate buffer (pH 2.0, $c = 0.2$ M/acetonitrile mixture solution (50/50 v/v)). The forward current corresponds to the oxidation of **PTZ** to **PTZ_{ox}** and the reverse current corresponds to the reduction of **PTZ_{ox}** to **PTZ**. In this method, the theoretical current ratio for a reversible system at 2τ and τ ($I_{r(2\tau)}/I_{f(\tau)}$) is 0.293^{32,34–36}.

The experimental current ratio ($I_{r(2\tau)}/I_{f(\tau)}$) obtained for **PTZ** is equal to 0.25, which is slightly less than the theoretical value but close to it. This result confirms the relative stability of oxidized **PTZ** (**PTZ_{ox}**) in the time scale of the experiment. Repeating this experiment for the oxidation of **PTZ** in the presence of **BSA** and measuring the current at 2τ and τ ($I_{r(2\tau)}/I_{f(\tau)}$) shows two important facts. First, the forward currents in these two experiments are exactly the same, and second, the reverse current ($I_{r(2\tau)}$) in the presence of **BSA** is zero. These results confirm that **PTZ_{ox}** is removed from the electrode surface due to its reaction with **BSA** on the time scale of the experiment.

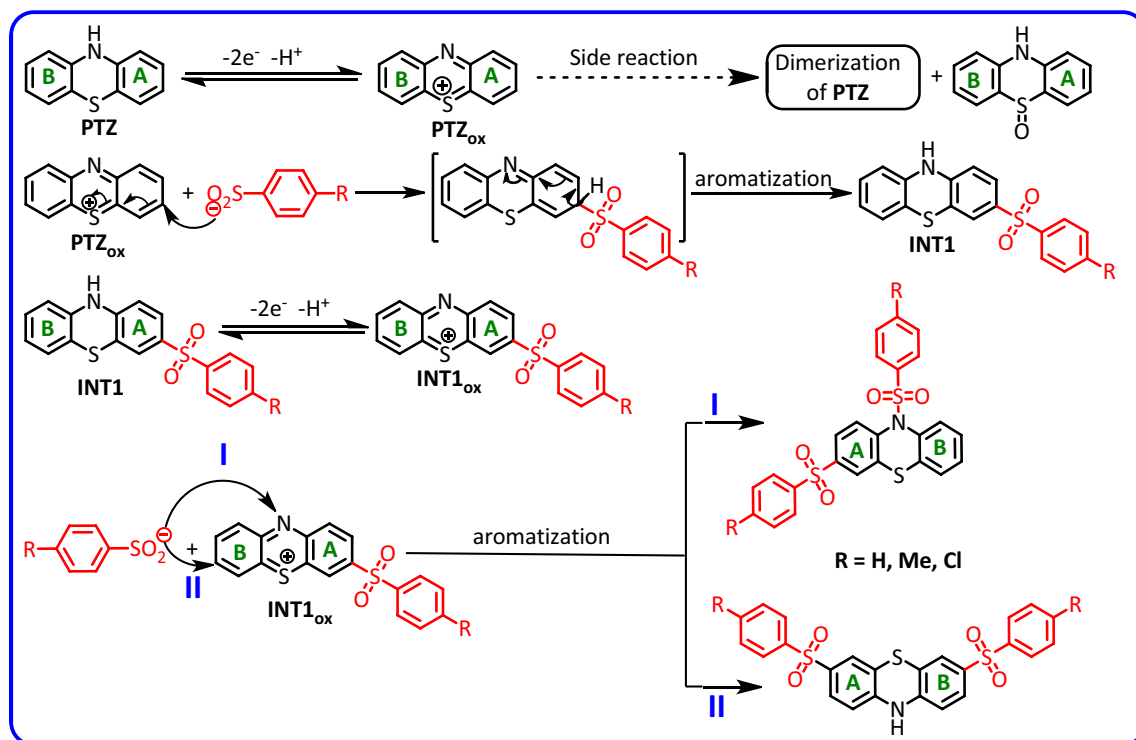


Figure 4. Suggested mechanism for electrochemical oxidation of **PTZ** in the presence of arylsulfinic acids.

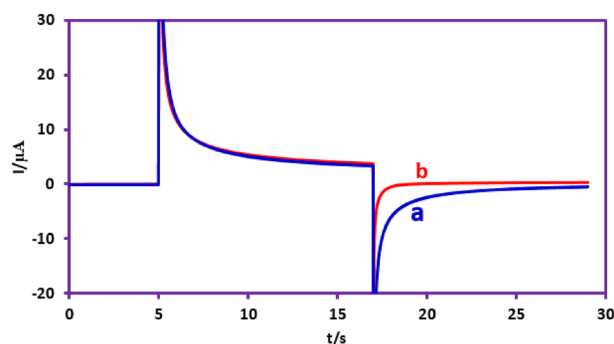


Figure 5. Double potential step chronoamperograms of 1.0 mM PTZ: (a) in the absence, (b) in the presence of 1.0 mM BSA. $E_1 = 0.20$ V vs. Ag/AgCl, E_2 (oxidation step) = 0.55 V vs. Ag/AgCl and E_3 (reduction step) = 0.40 V vs. Ag/AgCl. Solvent: phosphate buffer (pH 2.0, $c = 0.2$ M)/acetonitrile mixture (50/50 v/v). All experiments were performed at room temperature using a GC electrode.

Due to the fundamental difference in the structure of the synthesized products (3,10-bis(phenylsulfonyl)-10*H*-phenothiazine, **2a** and 3,7-bis(phenylsulfonyl)-10*H*-phenothiazine, **2b**), this section is dedicated to investigating the electrochemical behavior of the synthesized products **2a** and **2b**. Figure 6 curve a, shows the cyclic voltammogram of **2b**. The cyclic voltammogram displays a quasi-reversible redox process ascribed to the oxidation of **2b** to **2b_{ox}** and vice versa. Comparing the cyclic voltammogram of **2b** with that of PTZ (Fig. 6 curve b) shows that the oxidation potential of **2b** is about 140 mV more anodic than the PTZ oxidation potential. The peak shift can be expected due to the difference in the structure of **2b** (the presence of two electron withdrawing sulfonyl groups) with PTZ. In addition, the presence of two sulfonyl groups in the structure of **2b** has caused its oxidized form (**2b_{ox}**) to become more unstable than the oxidized form of PTZ (**PTZ_{ox}**) and thus participate in subsequent chemical reactions. As a result, the current of its cathodic peak (C_3) becomes lower than the current of cathodic peak of PTZ (C_1). Figure 6 curve d, shows the cyclic voltammogram of **2a**. In similar conditions, unlike the cyclic voltammogram of **2b**, the cyclic voltammogram of **2a** shows the presence of an irreversible process. The main reason for this difference is the attachment of a sulfonyl group to the nitrogen atom. This binding causes the two-electron oxidation of the **2a** to form a highly unstable **2a_{ox}** compound (Fig. 4).

According to the proposed mechanism in Fig. 4, the structure of the product formed via pathway II (for example **2b**) is similar to that of PTZ and therefore, its general electrochemical behavior should also be similar to PTZ. In Fig. 6, we studied and compared the cyclic voltammogram of product **2b** with the cyclic voltammogram of PTZ. Based on this, the redox reactions producing the anodic and cathodic peaks A_3 and C_3 is shown in Fig. 7. The electrochemical oxidation of **2a** was also studied (Fig. 6, curve d). Replacing the hydrogen atom in the PTZ molecule with a sulfinic group has a great effect on the stability of the oxidized product (**PTZ_{ox}**). The removal of the hydrogen atom attached to the nitrogen atom as a proton and giving its electron to the mother molecule causes the relative stability of the oxidized forms of molecules PTZ and **2b** (**PTZ_{ox}** and **2b_{ox}**). In contrast to these molecules, the replacement of the hydrogen atom with a sulfinic group in molecule **2a** has caused the oxidized molecule (**2a_{ox}**) to be in the dication form. This compound is very unstable and quickly participates in subsequent chemical processes such as ring cleavage^{37,38}, dimerization reactions^{39,40}, hydroxylation reactions^{41,42},

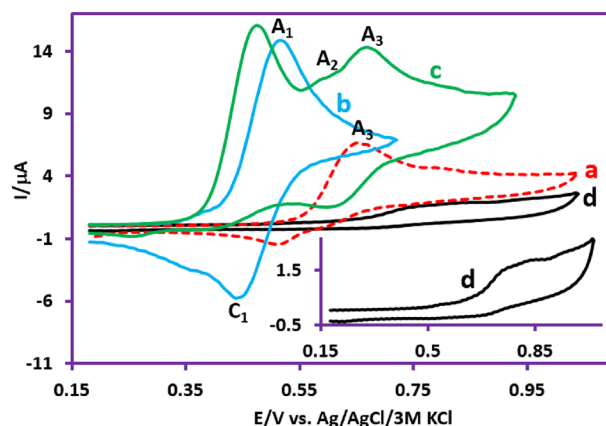


Figure 6. (a) Cyclic voltammogram of 1.0 mM **2b**. (b) Cyclic voltammogram of 1.0 mM PTZ. (c) Cyclic voltammogram of 1.0 mM PTZ in the presence of 1.0 mM BSA. (d) Cyclic voltammogram of 1.0 mM **2a**. Potential scan rate: 50 mV/s. Solvent: phosphate buffer (pH 2.0, $c = 0.2$ M)/acetonitrile mixture (50/50 v/v). Working electrode: glassy carbon electrode. All experiments were performed at room temperature.

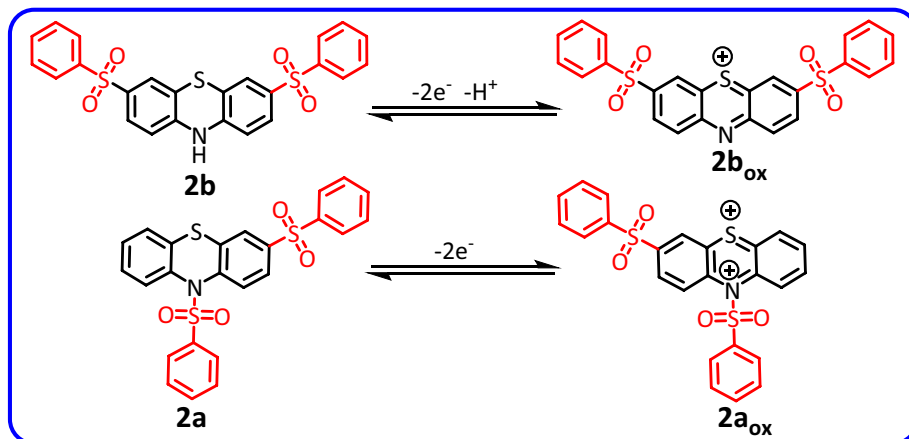


Figure 7. Suggested mechanism for electrochemical behavior of **2a** and **2b**.

hydrolysis^{43,44} and/or sulphoxide formation⁴⁵. The occurrence of these reactions makes the cyclic voltammogram of **2a** shows the behavior of an irreversible system.

In this part, it is necessary to consider the possibility of formation of different isomers in the oxidation of **PTZ** in the presence of arylsulfonic acids. Figure 8 shows the structures that may be formed in the oxidation of **PTZ** in the presence of arylsulfonic acids. The steric energy calculations show that due to the steric hindrance caused by the presence of two arylsulfonic groups in the *ortho* position to each other, it is not possible to form molecules such as I, X, XIV and XV.

As discussed earlier, it seems that due to the presence of sulfonium atom in **PTZ**_{ox} structure, beside nitrogen atom, C1 and C3 atoms are the most favorable sites for nucleophilic attack. Accordingly, the probability of formation of molecules IX, XII and XVII is very low and therefore they are excluded from the set of possible structures. It seems that the first nucleophilic attack leads to the formation of one of the following intermediates (**INTA**, **INTB** and **INTC**) shown in Fig. 9.

As discussed, the second oxidation step of the **INTA** leads to the corresponding dication, which is a very unstable compound and does not appear to be capable of conversion to our desired product (molecule III, **2a**). Therefore, we do not consider this pathway possible in the oxidation of **PTZ** in the presence of arylsulfonic acids. However, the second oxidation step of the intermediates **INTB** and **INTC** leads to the compounds I, III, VI, VII, XI and XVI. By removing compound I for the reasons mentioned earlier, the only remaining compound with the presence of a sulfonic group on the nitrogen atom is compound III (**2a**). By excluding, compounds I and III, the ¹H NMR spectrum of the product was compared with the simulated ¹H NMR spectra of compounds VI, VII, XI and XVI. This comparison shows that the experimental spectrum is the most consistent with the simulated spectrum for compound VI (Fig. 10).

Controlled potential coulometry

Controlled potential coulometry was carried out in a solution containing 0.25 mmol of **PTZ** and 0.5 mmol **BSA** in phosphate buffer (pH 2.0, *c* = 0.2 M/acetone nitrile solution mixture (50/50, v/v) at 0.55 V versus Ag/AgCl. In order to better understand what happens during coulometry, cyclic voltammograms of the electrolyzed solution were recorded during coulometry (Fig. 11). These voltammograms at different time intervals show that the peak A₁ current decreases in the progress of electrolysis. The second change observed in cyclic voltammograms is the appearance of peak A₂ and its relative increase with the progress of coulometry. Plotting the values of peak A₁ current versus the amount of electricity consumed in order to determine the number of electrons consumed in this process shows that peak A₁ disappears with the consumption of about 104 coulombs of electricity (Fig. 11, inset).

According to the electricity consumption and performing the necessary calculations, 4.1 electrons are assigned to each molecule of **PTZ**. This number is slightly higher than 4 due to electrolysis in an undivided cell. The number of electrons obtained in this experiment (*n* = 4) is consistent with that reported in Fig. 4. According to Fig. 4, two electrons are used to oxidize **PTZ** to **PTZ**_{ox} (peak A₁) and the other two electrons are used to oxidize intermediate **INT1** to **INT1**_{ox} (peak A₂). It should be noted that, the lack of increase in *I*_{PA3} and *I*_{PC3} during electrolysis is due to the insolubility of final products in electrolysis solution (see experimental section).

Constant current synthesis and optimization of effective parameters

In order to facilitate the synthesis of these compounds in a way that can be used by all researchers, in this section, the synthesis of these compounds in constant current mode has been examined and the effective parameters in improving the efficiency and purity of the products, such as applied current density, amount of electricity, solution pH, electrode material and solvent mixture are optimized by one factor at a time method. The current density is one of the most important parameters in electrochemical synthesis of organic and inorganic compounds, which affects the yield and purity. In this section, the electrochemical synthesis of products (**2a** and **2b**) was investigated at different current densities from 0.41 to 2.08 mA/cm² (Fig. 12, part I) while other parameters are kept constant (see the caption of Fig. 12). The results showed that the highest product yield (89%) was obtained at a current

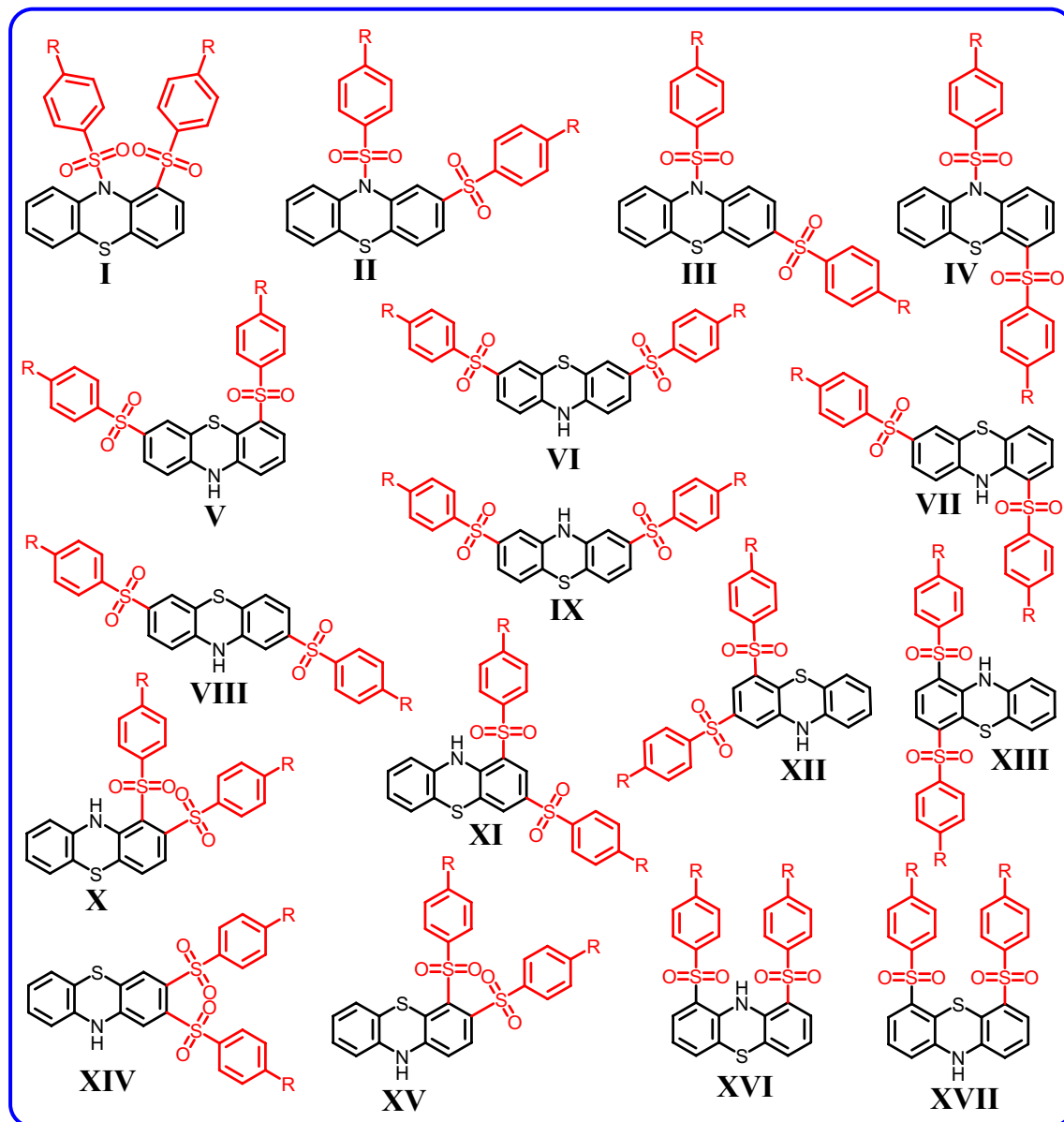


Figure 8. Possible structures in oxidation of PTZ in the presence of arylsulfonic acids.

density of 1.25 mA/cm^2 . At current densities less than 1.25 mA/cm^2 , the amount of overvoltage is not sufficient to oxidize PTZ and/or intermediates. On the other hand, at current densities higher than the optimal current density (1.25 mA/cm^2), oxidation of the solvent, supporting electrolyte and/or over-oxidation of the product will reduce the production yield (Fig. 12, part I). To optimize the amount of electricity, the electrochemical synthesis of **2a** and **2b** was investigated at different amount of electricity and at current density of 1.25 mA/cm^2 while other parameters are kept constant. The results showed that the highest product yield was obtained at $Q = 140 \text{ C}$. The higher amount of electricity consumed in the constant current method compared to the controlled potential method is due to the inherent difference of the two methods in the selective consumption of electricity.

The effect of solution pH on the yield and purity of products was also investigated (Fig. 12, part II). For this purpose water with different pH values of 1.0, 2.0, 6.0, 8.0 and 10.0/acetonitrile (50/50 v/v) solution mixtures are prepared. Phosphate buffer (0.2 M) was used to prepare solutions with pH values 2.0, 6.0 and 8.0. For pH = 1.0, perchloric acid solution (0.1 M) and for pH = 10.0, carbonate buffer (0.2 M) was used. Other conditions such as current density (1.25 mA/cm^2) and electricity consumption (140 C) were constant in all experiments. Figure 12, part II shows that the optimum pH is 2.0 for highest product yield. The instability of PTZ_{ox} in alkaline solutions and participation in side reactions such as dimerization^{10,39,40} and/or hydroxylation^{10,41,42} is the main reason for the low yield of the product in alkaline solutions. On the other hand, the one-electron oxidation of PTZ in highly acidic solutions¹⁰ and the instability of cation radicals along with nucleophile protonation, reduce the product yield in highly acidic solutions.

In this section, the effect of electrode materials on product efficiency is investigated and the results are given in Table 1. As can be seen, the highest product yield was achieved with carbon anode and stainless steel cathode

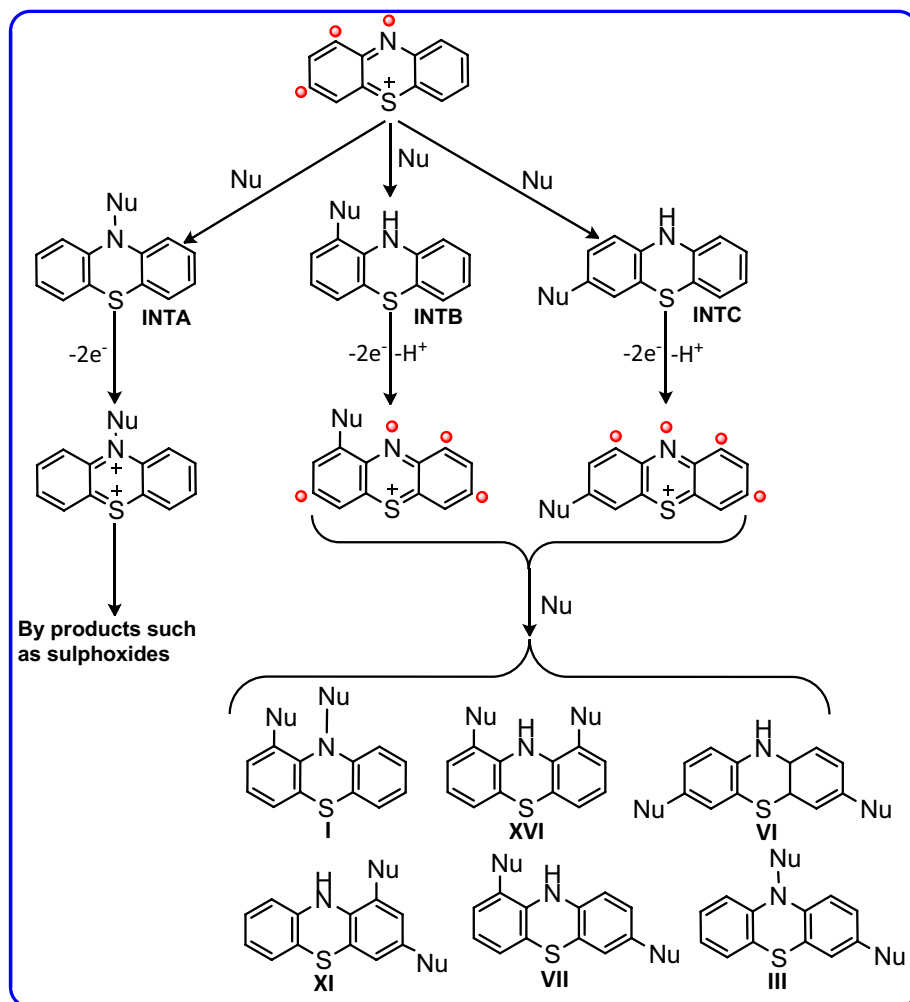


Figure 9. Possible pathways and products after attachment of the first arylsulfinic group.

in aqueous phosphate buffer (pH, 2.0, $c = 0.2M$)/acetonitrile mixture (50/50 v/v). The last optimization in this work was performed on the solvent system. The use of organic co-solvent is due to the low solubility of PTZ in water. Therefore, solvents such as ethanol and acetonitrile have been used as co-solvents. It should be noted that PTZ is easily soluble in acetone. But due to the unexpected reactivity of acetone as a solvent, this compound was not examined as a co-solvent.

The effect of solvent system on product yield is shown in Table 2. As can be seen, the highest product yield was achieved in aqueous phosphate buffer (pH, 2.0, $c = 0.2 M$)/acetonitrile mixture (50/50 v/v). It should be noted that increasing the percentage of acetonitrile in the mixture does not have a significant effect on the yield of the product. In addition, our research has shown that replacing ethanol with acetonitrile in the solvent mixture decreases yield. The decrease may be due to the low solubility of PTZ in ethanol. A large increase in the percentage of ethanol in the water/ethanol mixture increases the solubility of PTZ (slightly), but on the other hand, it causes a marked decrease in the solubility of the supporting electrolyte. Regarding the solution pH, it should be noted that increasing the pH from 2.0 decreases the yield of **2a** and **2b**. Increasing pH causes deprotonation of $PTZH^+$ and coupling reaction of PTZ with PTZ_{ox} (dimerization reaction)¹⁰. This reaction competes with the reaction between arylsulfinic acids and PTZ_{ox} . In other words, decreasing the pH causes the protonation of PTZ (formation of $PTZH^+$) and suppresses the dimerization reaction. It should be noted that due to the low basicity of arylsulfinate anions ($pK_a < 2.0$)⁴⁷, decreasing the pH does not have a significant effect on their nucleophilicity.

Conclusion

In this study, the electrochemical synthesis of five new phenothiazine derivatives (bis(phenylsulfonyl)-10H-phenothiazine derivatives) in water/acetonitrile mixture was carried out in a one-pot process through the electrochemical generation of phenothiazin-5-ium (PTZ_{ox}) in the presence of arylsulfinic acids. Our results show that two different types of products (bis(phenylsulfonyl)-10H-phenothiazine derivatives) are formed during the electrolysis: (1) Phenothiazine-sulfonamide-sulfone derivatives. In these products, one arylsulfinic group is attached to the nitrogen atom and the other group is attached to the carbon atom. (2) Phenothiazine-disulfone derivatives. In these products, both arylsulfinic groups are attached to carbon atoms. In addition to the controlled potential

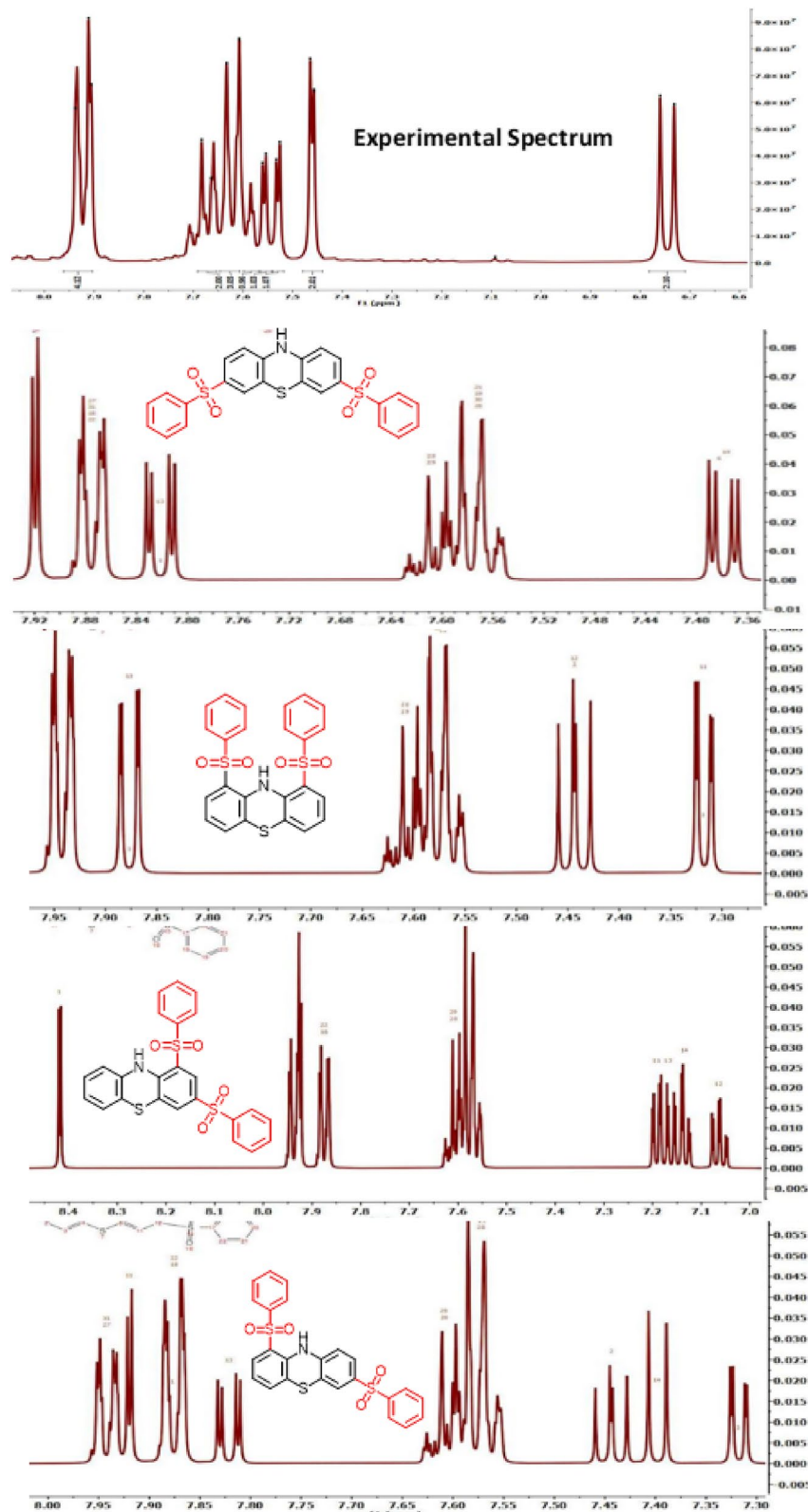


Figure 10. Experimental ^1H NMR spectrum of **2b** and simulated ^1H NMR spectra of different compounds.

method, the synthesis of these compounds by performing electrolysis in constant current mode has also been successful. In this research, a mechanism for the oxidation of PTZ in the presence of arylsulfinic acids was also proposed based on the data obtained from cyclic voltammetric, chronoamperometric and controlled-potential

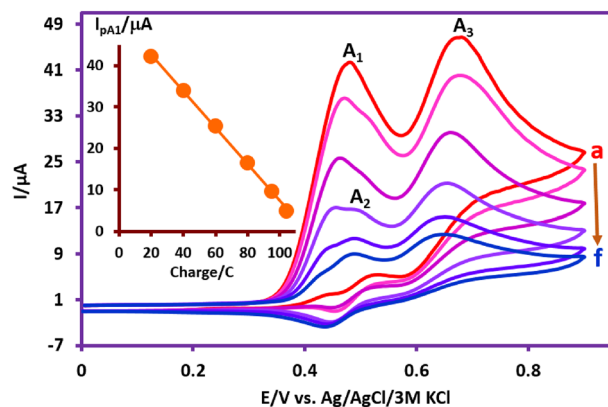


Figure 11. Cyclic voltammograms of 0.25 mmol PTZ in the presence of 0.5 mmol BSA during controlled-potential coulometry at 0.55 V vs. Ag/AgCl, in phosphate buffer (pH = 2.0, $c = 0.2$ M)/acetonitrile mixture (50/50 v/v). Cyclic voltammograms from a to f are: 20, 40, 60, 80, 95 and 104 C. Scan rate: 100 mV/s. Inset: Variation of A_1 peak current (I_{pA1}) vs. charge consumed. Working electrode: glassy carbon electrode. All experiments were performed at room temperature.

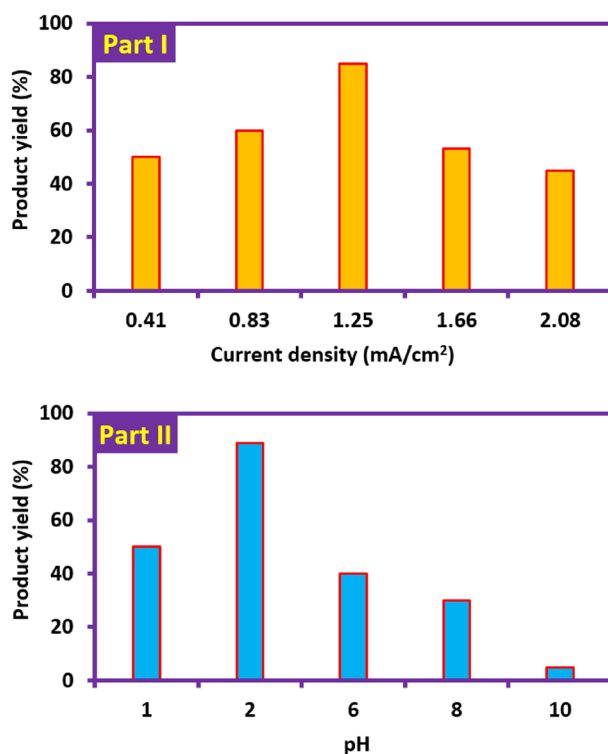
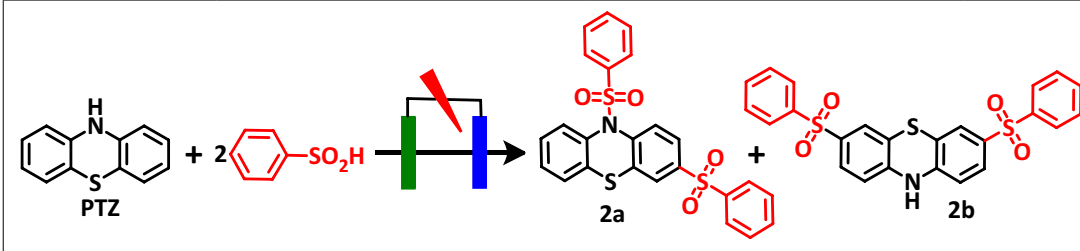


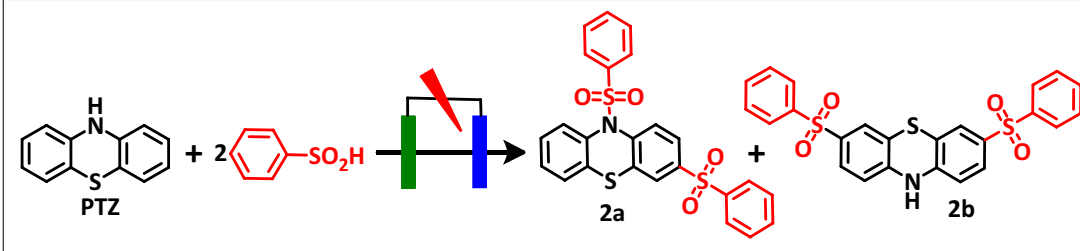
Figure 12. Part I: The effect of current density on the product yield (both **2a** and **2b**). The amounts of PTZ and BSA 0.25 and 0.5 mmol, respectively. $Q = 140$ C. Solvent: phosphate buffer (pH = 2.0, $c = 0.2$ M)/acetonitrile mixture (50/50 v/v). Anode and cathode material: carbon and stainless steel, respectively. Part II: The effect of solution pH on the yield of product. Applied current density: 1.25 mA/cm^2 . Other conditions are the same as part I. All experiments were performed at room temperature.

coulometric studies along with the structure of the synthesized products. This mechanism is depicted in Fig. 4. According to Fig. 4, PTZ is converted to the final product (bis(phenylsulfonyl)-10H-phenothiazine derivatives) through the *ECEC* mechanism. The insolubility of the final product in the electrolysis solution is one of the factors that prevent the re-oxidation of the final product. Finally, we hope that the synergistic effect of the groups added to the phenothiazine molecule will intensify the medicinal properties and/or reduce the side effects of the synthesized molecules.



Entry	Anode	Cathode	Yield (%) ^{a,b}
1	carbon	stainless steel	89
2	stainless steel	stainless steel	20
3	stainless steel	carbon	35
4	titanium	stainless steel	50
5	Ti/ β -PbO ₂ /CeO ₂ ^c	stainless steel	75

Table 1. Optimization of electrode material for the synthesis of **2a** and **2b**. ^aThe yield reported is the sum of yields of products **2a** and **2b**. ^bApplied current density: 1.25 mA/cm². Electricity consumption: 140 C. Solvent: phosphate buffer (pH = 2.0, *c* = 0.2 M)/acetonitrile mixture (50/50 v/v). ^cThe electrode was fabricated according to the procedure reported in reference⁴⁶.



Entry	Organic co-solvent	Aqueous solution, pH	Yield (%) ^{a,b}
1	EtOH	phosphate buffer (pH, 2.0, <i>c</i> = 0.2 M)	20
2	CH ₃ CN	phosphate buffer (pH, 2.0, <i>c</i> = 0.2 M)	89
3	–	phosphate buffer (pH, 2.0, <i>c</i> = 0.2 M)	no reaction
4	CH ₃ CN	phosphate buffer (pH, 6.0, <i>c</i> = 0.2 M)	40

Table 2. Optimization of the solvent system for the synthesis of **2a** and **2b**. ^aThe yield reported is the sum of yields of products **2a** and **2b**. ^bApplied current density: 1.25 mA/cm². Electricity consumption: 140 C. Solvent: phosphate buffer (pH = 2.0 or 6.0, *c* = 0.2 M)/organic solvent mixture (50/50 v/v). Anode: carbon. Cathode: stainless steel.

Data availability

All data generated or analyzed during this study are included in this published article.

Received: 30 October 2023; Accepted: 2 February 2024

Published online: 21 February 2024

References

1. Heard, D. M. & Lennox, A. Electrode materials in modern organic electrochemistry. *Angew. Chem. Int. Ed.* **59**, 18866–18884 (2020).
2. Leech, M. C. & Lam, K. A. practical guide to electrosynthesis. *Nat. Rev. Chem.* **6**, 275–286 (2022).
3. Zivari-Moshfegh, F., Khoram, M. M. & Nematollahi, D. Green electrochemical synthesis of silver sulfadiazine microcrystals. *RSC Adv.* **9**, 24105–24109 (2019).
4. Lodarski, K. *et al.* Discovery of butyrylcholinesterase inhibitors among derivatives of azaphenothiazines. *J. Enzyme Inhib. Med. Chem.* **30**, 98–106 (2015).
5. Pluta, K., Morak-Młodawska, B. & Jeleń, M. Recent progress in biological activities of synthesized phenothiazines. *Eur. J. Med. Chem.* **46**, 3179–3189 (2011).
6. Jaszczyszyn, A. *et al.* Chemical structure of phenothiazines and their biological activity. *Pharmacol. Rep.* **64**, 16–23 (2012).
7. Mentré, F. *et al.* Dose regimen of favipiravir for Ebola virus disease. *Lancet Infect. Dis.* **15**, 150–151 (2015).
8. Aktaş, A., Tüzün, B., Aslan, R., Sayin, K. & Ataseven, H. New anti-viral drugs for the treatment of COVID-19 instead of favipiravir. *J. Biomol. Struct. Dyn.* **39**, 7263–7273 (2021).
9. Jiang, Y., Xu, K. & Zeng, C. Use of electrochemistry in the synthesis of heterocyclic structures. *Chem. Rev.* **118**, 4485–4540 (2017).

10. Mohamadighader, N., Nematollahi, D. & Saraei, M. A. comprehensive study on electrochemical oxidation of phenothiazine in water-acetonitrile mixture: Electrosynthesis of phenothiazine dimers. *Electrochim. Acta* **425**, 140706 (2022).
11. Scott, K. A. & Njardarson, J. T. Analysis of US FDA-approved drugs containing sulfur atoms. In *Sulfur Chemistry* 1–34 (Springer, 2019).
12. Zhou, J. *et al.* Extended phenothiazines: synthesis, photophysical and redox properties, and efficient photocatalytic oxidative coupling of amines. *Chem. Sci.* **13**, 5252–5260 (2022).
13. Padhy, H. J. *et al.* Synthesis and applications of low-bandgap conjugated polymers containing phenothiazine donor and various benzodiazole acceptors for polymer solar cells. *J. Polym. Sci. Part A Polym. Chem.* **48**, 4823–4834 (2010).
14. Ullah, A. *et al.* Novel phenothiazine-based self-assembled monolayer as a hole selective contact for highly efficient and stable p-i-n perovskite solar cells. *Adv. Energy Mater.* **12**, 2103175 (2022).
15. Tozkoparan, B., Küpeli, E., Yeşilada, E. & Ertan, M. Preparation of 5-aryl-3-alkylthio-1,2,4-triazoles and corresponding sulfones with antiinflammatory–analgesic activity. *Bioorganic Med. Chem. Lett.* **15**, 1808–1814 (2007).
16. Hwang, S. H. *et al.* Synthesis and structure–activity relationship studies of urea-containing pyrazoles as dual inhibitors of cyclooxygenase-2 and soluble epoxide hydrolase. *J. Med. Chem.* **54**, 3037–3050 (2011).
17. Kudryavtsev, K. V., Bentley, M. L. & McCafferty, D. G. Probing of the *cis*-5-phenyl proline scaffold as a platform for the synthesis of mechanism-based inhibitors of the *Staphylococcus aureus* sortase SrtA isoform. *Bioorganic Med. Chem. Lett.* **17**, 2886–2893 (2009).
18. Guruswamy, B., Arul, R. K., Chaitan, M. V. S. R. K. & Darsi, S. S. P. K. Synthesis and biological evaluation of novel β -hydroxy benzimidazolyl sulfone fluoroquinolones by selective oxidation using ammonium molybdate catalysed H_2O_2 . *Eur. J. Chem.* **4**, 329–335 (2013).
19. Al-Said, M. S., Ghorab, M. M. & Nissan, Y. M. Dapson in heterocyclic chemistry, part VIII: Synthesis, molecular docking and anticancer activity of some novel sulfonylbiscompounds carrying biologically active 1,3-dihydropyridine, chromene and chromenopyridine moieties. *Chem. Cent. J.* **6**, 1–14 (2012).
20. Kamble, R. B., Chavan, S. S. & Suryavanshi, G. An efficient heterogeneous copper fluorapatite (CuFAP)-catalysed oxidative synthesis of diaryl sulfone under mild ligand- and base-free conditions. *N. J. Chem.* **43**, 1632–1636 (2019).
21. Anderson, R., Groundwater, P. W., Todd, A. & Worsley, A. *Antibacterial Agents: Chemistry, Mode of Action, Mechanisms of Resistance and Clinical Applications* (John Wiley & Sons, 2012).
22. Shoaib Ahmad Shah, S., Rivera, G. & Ashfaq, M. Recent advances in medicinal chemistry of sulfonamides. Rational design as anti-tumoral, anti-bacterial and anti-inflammatory agents. *Mini Rev. Med. Chem.* **13**, 70–86 (2013).
23. Scozzafava, A., Owa, T., Mastrolorenzo, A. & Supuran, C. T. Anticancer and antiviral sulfonamides. *Curr. Med. Chem.* **10**, 925–953 (2003).
24. Supuran, C. T., Casini, A. & Scozzafava, A. Protease inhibitors of the sulfonamide type: Anticancer, antiinflammatory, and antiviral agents. *Med. Res. Rev.* **23**, 535–558 (2003).
25. Rakesh, K. P. *et al.* Recent development of sulfonyl or sulfonamide hybrids as potential anticancer agents. *Med. Chem.* **18**, 488–505 (2018).
26. Pant, S. M. *et al.* Design, synthesis, and testing of potent, selective hepsin inhibitors via application of an automated closed-loop optimization platform. *J. Med. Chem.* **61**, 4335–4347 (2018).
27. Nishioka, H., Tooi, N., Isobe, T., Nakatsuji, N. & Aiba, K. BMS-708163 and Nilotinib restore synaptic dysfunction in human embryonic stem cell-derived Alzheimer's disease models. *Sci. Rep.* **6**, 33427 (2016).
28. Pennington, L. D. *et al.* Discovery and structure-guided optimization of diarylmethanesulfonamide disruptors of glucokinase–glucokinase regulatory protein (GK–GKRP) binding: Strategic use of a N→S (nN→ σ^* S-X) interaction for conformational constraint. *J. Med. Chem.* **58**, 9663–9679 (2015).
29. Gillman, K. W. *et al.* Discovery and evaluation of BMS-708163, a potent, selective and orally bioavailable γ -secretase inhibitor. *ACS Med. Chem. Lett.* **1**, 120–124 (2010).
30. Sugimoto, H. *et al.* An orally bioavailable small molecule antagonist of CRTH2, ramatroban (BAY u3405), inhibits prostaglandin D2-induced eosinophil migration in vitro. *J. Pharmacol. Exp. Ther.* **305**, 347–352 (2003).
31. Lafferty, J. J., Garvey, E., Nodiff, E. A., Thompson, W. E. & Zirkle, C. L. The synthesis of phenothiazines. VII. Methyl- and arylsulfonylation of phenothiazine and its 10-substituted derivatives. *J. Org. Chem.* **27**, 1346–1351 (1962).
32. Bard, A. J. & Faulkner, L. R. *Electrochemical Methods: Fundamentals and Applications* (Wiley, 2001).
33. Nematollahi, D., Joudaki, M., Khazalpour, S. & Pouladi, F. Electrochemical oxidation of sulfonic acids: Efficient oxidative synthesis of diaryl disulfones. *J. Electrochem. Soc.* **164**, G65–G70 (2017).
34. Zivari-Moshfegh, F., Javanmardi, F. & Nematollahi, D. A comprehensive electrochemical study on anti-tuberculosis drug rifampicin. Investigating reactions of rifampicin-quinone with other anti-tuberculosis drugs, isoniazid, pyrazinamide and ethambutol. *Electrochim. Acta* **457**, 142487 (2023).
35. Zivari-Moshfegh, F. & Nematollahi, D. An eco-friendly electrochemical process for the formation of a new desloratadine derivative and its antibacterial susceptibility. Report of a new type of ortho-quinhydrone complex. *Electrochim. Acta* **421**, 140518 (2022).
36. Zivari-Moshfegh, F. & Nematollahi, D. New insights into co-administration of anti-tuberculosis drug rifampicin with acetaminophen and vitamin C: Strong electrochemical evidence for the detoxification. *J. Electrochem. Soc.* **170**, 095501 (2023).
37. Varmaghani, F., Nematollahi, D., Mallakpour, S. & Esmaili, R. Electrochemical oxidation of 4-substituted urazoles in the presence of arylsulfonic acids: An efficient method for the synthesis of new sulfonamide derivatives. *Green Chem.* **14**, 963–967 (2012).
38. Varmaghani, F. & Nematollahi, D. Electrochemical study of 1,2-dihydropyridazine-3,6-dione in protic and aprotic solvents: Oxidative ring cleavage and reduction. *Electrochim. Acta* **56**, 6089–6096 (2011).
39. Salehzadeh, H., Nematollahi, D. & Rafiee, M. Electrochemical dimerization of 4-methylesculetin: Synthesis and kinetic study of a highly-oxygenated dimer. *J. Electroanal. Chem.* **650**, 226–232 (2011).
40. Shahparast, S., Nematollahi, D., Sharafi-Kolkeshvandi, M. & Goljani, H. Direct electrochemical dimerization of N, N'-diphenylbenzidine. *J. Electrochem. Soc.* **166**, G47 (2019).
41. Nematollahi, D., Shayani-Jam, H., Alimoradi, M. & Niroomand, S. Electrochemical oxidation of acetaminophen in aqueous solutions: Kinetic evaluation of hydrolysis, hydroxylation and dimerization processes. *Electrochim. Acta* **54**, 7407–7415 (2009).
42. Sour, Z., Masoudi Khoram, M., Nematollahi, D., Mazloum-Ardakani, M. & Alizadeh, H. A. green protocol for the electrochemical synthesis of a fluorescent dye with antibacterial activity from imipramine oxidation. *Sci. Rep.* **12**, 4921 (2022).
43. Beiginejad, H. & Nematollahi, D. Electrochemical oxidation of 2, 5-diethoxy-4-morpholinooaniline in aqueous solutions. *Electrochim. Acta* **114**, 242–250 (2013).
44. Beiginejad, H., Nematollahi, D., Varmaghani, F. & Bayat, M. Efficient factors on the hydrolysis reaction rate of some *para*-aminophenol derivatives in acidic pHs. *J. Electrochem. Soc.* **160**, H469 (2013).
45. Blankert, B. *et al.* Electrochemical, chemical and enzymatic oxidations of phenothiazines. *Electroanalysis* **17**, 1501–1510 (2005).
46. Zhang, C., Liu, J. & Chen, B. Effect of CeO_2 and graphite powder on the electrochemical performance of Ti/PbO₂ anode for zinc electrowinning. *Ceram. Int.* **44**, 19735–19742 (2018).
47. Jamshidi, M., Nematollahi, D., Bayat, M. & Salahifar, E. Unsymmetrical diaryl sulfones through electrochemical oxidation of fast violet B in the presence of aryl sulfonic acids. *J. Electrochem. Soc.* **163**, G211–G218 (2016).

Acknowledgements

The authors acknowledge the Bu-Ali Sina University Research Council and Center of Excellence in Development of Environmentally Friendly Methods for Chemical Synthesis (CEDEFMCS) for their support of this work.

Author contributions

N.M. investigation, conceptualization, methodology, writing—original draft. F.Z.M. investigation, conceptualization, methodology, writing—original draft. D.N. writing—review & editing, supervision, project administration.

Competing interests

The authors declare no competing interests.

Additional information

Correspondence and requests for materials should be addressed to D.N.

Reprints and permissions information is available at www.nature.com/reprints.

Publisher's note Springer Nature remains neutral with regard to jurisdictional claims in published maps and institutional affiliations.



Open Access This article is licensed under a Creative Commons Attribution 4.0 International License, which permits use, sharing, adaptation, distribution and reproduction in any medium or format, as long as you give appropriate credit to the original author(s) and the source, provide a link to the Creative Commons licence, and indicate if changes were made. The images or other third party material in this article are included in the article's Creative Commons licence, unless indicated otherwise in a credit line to the material. If material is not included in the article's Creative Commons licence and your intended use is not permitted by statutory regulation or exceeds the permitted use, you will need to obtain permission directly from the copyright holder. To view a copy of this licence, visit <http://creativecommons.org/licenses/by/4.0/>.

© The Author(s) 2024